Rate Mechanism of Plasticity in the Crystalline Component of Semicrystalline Nylon 6

L. Lin† and A. S. Argon*

Massachusetts Institute of Technology, Cambridge, Massachusetts 02139

Received June 24, 1994; Revised Manuscript Received August 12, 1994®

ABSTRACT: The rate mechanism of crystal plasticity was studied in quasi-single crystalline (QSC) Nylon 6 prepared by plane strain compression in a channel die to equivalent extensional strains on the order of 1.39. Specimens of such highly oriented material were probed in simple shear experiments on the (001)[010] and (100)[010] monoclinic chain slip systems by means of strain rate change experiments in the temperature range of 255–366 K. These experiments demonstrated that while there is a well developed glass transition in the shear moduli of the material there is no corresponding transition in the plastic resistances, indicating that the plastic behavior of the QSC material is derived entirely from the crystalline component. Analysis of the experiments with reference to dislocation mechanics has disclosed that the plastic shear resistance for the chain slip systems is made up of several components. These include an athermal component due to random internal stresses of misfit, a lattice resistance, most probably affecting only the screw dislocations, and a terminal nonhardening flow resistance due to close range interaction of these dislocations with a family of small crystalline packing imperfections such as chain crossovers, slack pockets, etc. Activation analysis has indicated that the activation volumes Δv^* governing this interaction are linearly dependent on stress, resulting at zero stress in $\Delta v^* = 6 \times 10^{-21}$ cm^3 for the (001)[010] chain slip system and 2.73×10^{-21} cm^3 for the (100)[010] chain slip system. Moreover, from the stress level where the activation volume vanishes athermal overall shear resistances of 8.2% and 14.2% of the respective shear moduli of the (001)[010] and (100)[010] slip systems are obtained respectively. Experiments were also carried out on untextured Nylon 6 for purposes of comparison. These gave results intermediate to those of the chain slip systems.

1. Introduction

The phenomenology and mechanisms of plastic deformation in semicrystalline polymers, and particularly in high density polyethylene (HDPE), have been of considerable interest since the pioneering studies of Peterlin,[1] Ward,[2] Keller,[3] and their co-workers. Much of this research has recently been reviewed by us elsewhere.[4] The vast majority of these early investigations and even most of the present ones have remained either at the phenomenological level of studying the kinematics of the process in relation to the complex morphology or to describe its stress conditions by global multiaxial yield criteria. On the fine structure scale a vast number of experiments concentrated, by means of transmission electron microscopy, on the behavior of electron transparent thin films lacking the important constraints of bulk deformation (for a brief assessment see ref 4). The few exercises with a deeper commitment remained of a theoretical nature involving lattice defects[5–7] or explored kinetics of dislocation motion.[8–10] Clearly, much of the difficulty in providing a definitive description of phenomena or a comprehensive theory can be ascribed to the complex morphology of the material in bulk and the inadequate understanding of the topology of individual chain molecules weaving in and out of the lamellar crystallites at the crystal/amorphous interfaces. Much painstaking long term research of this subject by Mandelkern and co-workers has been summarized recently by him in a succinct review.[11] Some recent investigations of the large strain deformation behavior of HDPE and Nylon 6 by Argon and associates, particularly those studies related to plane strain compression,[12–17] provide a stimulus for a renewed attack on the possible mechanistic interpretation of plasticity in the crystalline component of semicrystalline polymers. While these new developments, on which the present study is based, make some definitive statements possible for the highly textured quasi-single crystalline material, questions still remain on the degree of applicability of these to the initial spherulitic morphology.

The principal development that makes a renewed attack on the mechanism of crystal plasticity possible is the very recent realization that in the highly textured material of quasi-single crystal (QSC) character that results from plane strain compression flow of HDPE and Nylon 6 to equivalent strains of 1.86 and 1.39, respectively, the molecules in the amorphous components are as highly aligned as those in the crystalline components,[12–15] where, moreover, the amorphous component often has remarkable symmetry registry with the crystalline component.[16] This gives rise to a fine scale dispersal of the amorphous component into the crystalline component, resulting in a much weaker differentiation between these components and the establishment of a remarkable degree of long range crystallike lateral coherence in the flow direction (direction of chain alignment). As already noted by Young[18] and more recently by Argon and associates[14,15] such textured QSC material serves well as an attractive vehicle for the experimental study of crystallographic slip resistance. We will demonstrate in the present study its remarkable utility in even more definitive studies of the kinetics of slip processes with very clear implications for dislocation mobility in polymer single crystals.

In the course of the determination of resistances of specific slip systems in HDPE[14] and Nylon[15] a strong normal stress dependence of the shear resistance was found on all slip systems, but particularly in the case of the two prominent chain slip systems in Nylon 6. There, in the principal chain slip system (001)[010] in which the hydrogen bonds lie in the slip plane, this dependence ($d\tau/d\sigma_n$) was found to be 0.13 but was more than twice as high at 0.28 for the second most prominent chain slip system of (100)[010] where the hydrogen bonds cut across the slip system. In HDPE this normal stress dependence was

* To whom all correspondence should be addressed.
† Present address: Marshall Laboratories of Research and Development, DuPont Co., Philadelphia, PA 19146.
® Abstract published in *Advance ACS Abstracts*, October 1, 1994.

0024-9297/94/2227-6903$04.50/0

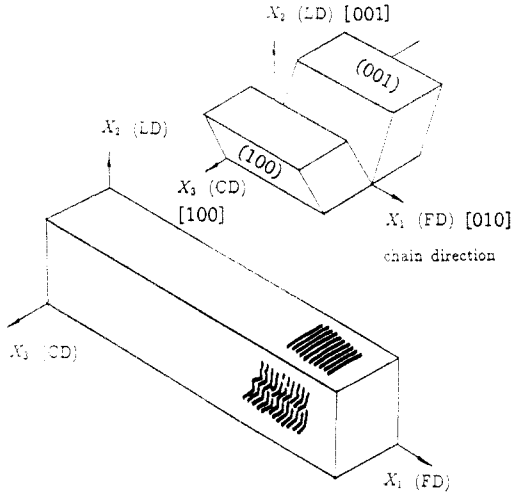

Figure 1. Principal coordinates of the quasi-single crystalline (QSC) textured Nylon 6 resulting from plane strain compression in a channel die to an equivalent strain of 1.39. The inset shows the symmetrical bimodal distribution of the monoclinic crystallographic domains.

found to be of a similarly high order even though in that case there is no hydrogen bonding across the slip planes. Thus, because of its stronger slip resistance anisotropy, Nylon 6 was chosen for the present study of the kinetics of crystallographic chain slip. The present investigation was carried out in simple shear on QSC Nylon 6 prepared by plane strain compression to an equivalent strain of about 1.39. In addition, for comparison purposes, the behavior of untextured initially spherulitic, Nylon 6 was also studied with the same methodology. The results will be interpreted in light of well-known forms of activation analysis of crystallographic slip arising from motion of dislocations.

2. Experimental Procedure

2.1. Textured Quasi-Single Crystalline Nylon 6. The material used in this study was Nylon 6 (Capron 8200 extracted, Allied Corp.). The weight-average molecular weight of the untextured material was 32 600, and the ratio of the weight-average to number-average molecular weight was 1.80. After plane strain compression[15] to a ratio of 4.0 (ϵ_e = 1.39) in a deep channel die apparatus at 170 °C and annealing at 195 °C in a vacuum oven for 24 h, the material was found to be highly textured and the crystallinity had changed from 38.5% to 44.3%. Wide-angle (WAXS) and small-angle X-ray scattering (SAXS) characterizations of this textured material have been described in detail elsewhere.[12,15] It was found that the overwhelmingly dominant crystalline form of the material was α. The orientation axes X_1, X_2, and X_3 of the textured materials with respect to the flow direction (FD), loading direction (LD), and constraint direction (CD) of the channel die equipment are illustrated in Figure 1.

The figure also shows the principal axes of the quasi-single crystalline material resulting from the plane strain compression, in the framework of the deformation axes X_1, X_2, and X_3. The planes of the principal chain slip system (001)[010] have a normal ($\vec{c}$) parallel to the X_2 axis, with the chain axes lying parallel to [010] (or [0140] because of the very long lattice periodicity). The planes of the second best chain slip system of (100)[010], in the monoclinic symmetry of this crystal structure, have normals ($\vec{b}$) that make an angle of 69° with the $\vec{c}$ axis. During the plane strain compression the overall population of deforming and rotating crystalline lamellae partition into two equal subpopulations, with their $\vec{b}$ axes making ±69° angles with the $\vec{c}$ direction which on the average is parallel to the X_2 deformation axis. The microstructural scale of these partitioned domains is as yet undetermined.

Figure 1 also shows a sketch of the morphological texture of the resulting long period of alternately layered crystalline lamellae and intervening amorphous slabs which have a straight appearance when viewed from the X_2 direction and a corrugated appearance when viewed from the X_3 directions. This morphology results in SAXS patterns which are in the form of a pair of spots when the material is viewed from the X_2 (LD) direction and a pair of straight elongated streaks normal to the X_1 direction when the material is viewed from the X_3 direction. That such a streaked pattern is a result of a randomly wavy shear in the X_1 direction of crystalline lamellae of relatively constant thickness has been discussed in some detail by Song et al.[19] (albeit in HDPE). Thus, unlike in HDPE where the plane strain compression results in a QSC macro slab, having the same orthorhombic symmetry, the same deformation process in the monoclinic Nylon 6 results in an equally partitioned set of aligned monoclinic quasi-crystalline domains. These collectively give only a material of orthotropic symmetry in which the symmetry axes X_1, X_2, and X_3 now coincide with the symmetry axes of the plane strain compression apparatus.

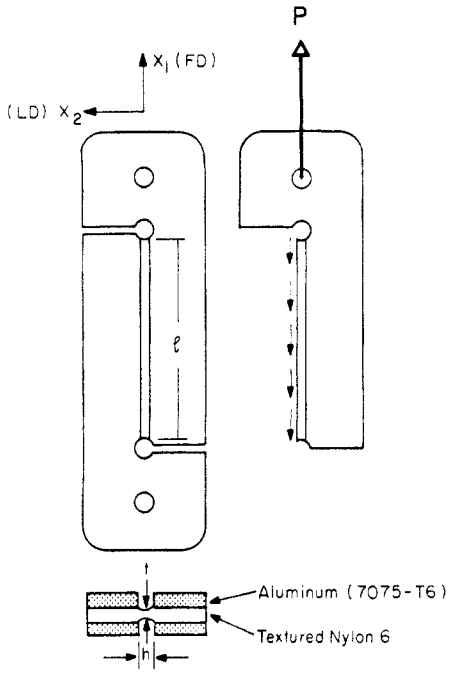

Figure 2. Sketch showing the simple shear arrangement for the QSC material.

The dimensions of the textured blocks resulting from the plane strain compression were 76 × 15 × 10 mm. Since Nylon is hygroscopic and the absorbed water affects its deformation resistance in an important way,[20] the processed blocks were always kept in hermetically sealed "Ziplock" bags and were removed only for short periods of sample preparation and experimentation which never exceeded a total period of 5 h. Thus, while the water content in the material has not been specifically determined or controlled, it is considered to be relatively uniform and constant in all experiments. The full details of preparation of the textured material can be found elsewhere.[21]

2.2. Simple Shear Tests. As stated above, the kinetics of crystallographic shear experiments were carried out in simple shear with no lateral stress acting across the slip planes. Figure 2 shows the shape and relative dimensions of the specimens for the simple shear test used in this study. Slices were cut from the highly textured QSC Nylon 6 of orthotropic symmetry by precision milling machines in a special way so that the desired crystallographic slip direction was parallel to the applied loads and the normal of the desired crystallographic plane was in the plane of the paper. Thus, the X_1 simple shear loading axis was always parallel to the flow direction (FD), X_1, of the plane strain compression axis, i.e., the molecular $\vec{b}$ axis. In the present study the (001) plane and the orthotropic (100) plane (making equal angles of 21° with the two possible sets of actual crystallographic (100) planes of the monoclinic system) were the shear planes, respectively. The simple shear experiments were also performed on untextured Nylon 6 for comparison with textured material.

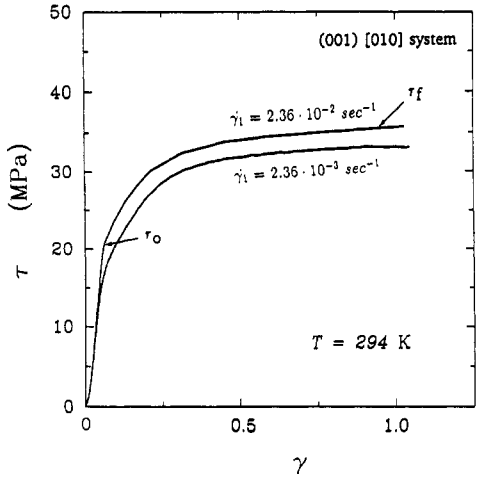

Figure 3. Two simple shear stress–strain curves at two different strain rates probing the QSC material on the monoclinic (001)-[010] chain slip system at room temperature.

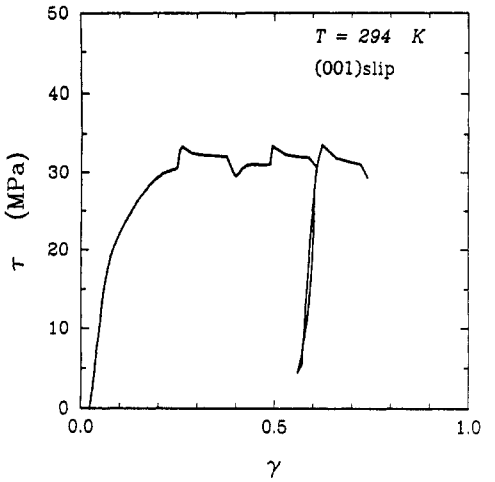

Figure 4. Simple shear stress–strain curve of the monoclinic (001)[010] system at room temperature showing apparent hardening, effect of abrupt change in strain rate, unloading, and reloading.

Each thin slab of the machined samples was glued between two pieces of high strength aluminum (7075-T6) by methacrylate adhesive (Plexus MA310 manufactured by ITW Devcon Co.). The final shape was prepared on a precision milling machine. The slots on each side of the specimen were aligned well with the holes, where a pair of concentrated forces were applied through high strength steel pins to enforce the deformation.

Problems of simple shear experiments can be reduced to a minimum when the test is designed appropriately. G'Sell et al.[22] showed that, by means of careful dimensional control and accuracy of specimen preparation in simple shear experiments, stray normal stresses acting across shear planes and end effects can be reduced to negligible levels when the ratio of shear length l to shear gap thickness h of a specimen (see Figure 2) is made larger than 15. Moreover, plastic wrinkling and other unwanted deformations, which could be present in shearing of thin polymer films,[23-25] should not occur when the ratio of the shear thickness, t, to shear height, h, of a specimen is equal to or larger than 0.75. These dimensional ratios were based on typical material characteristics such as $(d\tau/d\gamma)/E = 0.01$ (ratio of strain hardening rate in shear to Young's modulus) and $\nu = 0.35$ (Poisson's ratio). In the present work, the ratios l/h and t/h were at least 19 and 0.8, respectively, so that no unwanted stray effects were encountered.

The simple shear tests were performed on an Instron (Model 4201) machine, equipped with an environmental chamber for temperature control. The chamber had a temperature range from −72 to 200 °C. Experiments were performed at temperatures between 255 and 366 K and at shear strain rates between 2.36×10^{-3} and 2.36×10^{-2} s^{-1}. Instron Series IX software was used to collect force vs displacement data.

Since the experiments were done in an environmental chamber and used relatively compliant pull rods and pins in the loading train, the external displacement measurements made to calculate shear strain levels required corrections to be made.

To probe the rate mechanism of plastic shear by well established methods of activation analysis which we will discuss in section 4.3 below, strain rate change experiments were conducted by making sudden changes in crosshead velocity and by recording the resulting jump in the plastic shear resistance.

3. Experimental Results

3.1. Monoclinic (001)[010] Slip System. Two stress–strain curves in simple shear probing the monoclinic (001)-[010] slip system are given in Figure 3. The two tests were carried out at different shear strain rates a decade apart, at 2.36×10^{-3} and 2.36×10^{-2} s^{-1}, respectively. These two stress–strain curves, generated at room temperature, are quite representative of the nature of the simple shear experiment on the QSC Nylon 6 and of the orthotropic (100)[010] experiment, attempting to probe the actual monoclinic (100)[010] slip systems in the testing range of temperature and strain rate.

For small strains, the stress–strain response is linear and elastic. Transition to plastic behavior occurs relatively smoothly but in a readily recognizable form at a shear stress τ_0, which was determined by a simple construction involving the intersection of the straight elastic loading line and a power-law fit to the nonlinear plastic response curve, discussed in more detail earlier.[15] Between the initial yield to the plateau of fully developed plastic shear with no hardening is a relatively protracted transition region of increasing plastic resistance that may extend typically over a plastic shear strain of roughly 0.2. The vertical offset in the flow stress due to the increased strain rate is independent of strain (or flow stress) in the plateau region.

Figure 4 shows the effect of a sudden strain rate change on the flow stress in the plateau region of unrestricted shear flow and the effect of unloading and reloading. After the stress reached its plateau level, the applied strain rate was suddenly changed by a factor of 10 from its initial level at 2.36×10^{-3} s^{-1}. Then after a new condition of steady flow was achieved, the rate was changed back to 2.36×10^{-3} s^{-1} and increased once again back to 2.36×10^{-2} s^{-1}. This was followed by unloading and reloading at the high rate of 2.36×10^{-2} s^{-1}. The figure shows that there are overshoots in stress upon a sudden increment in strain rate before the stress reaches a new stable plateau, both when the strain rate is changed upward or downward during the deformation process. The slope of the unloading curve is markedly steeper than the initial linear loading curve. This is also the case for the reloading curve. The fact that the reloading curve has a higher slope than the initial loading curve indicates the development of a plastic shear-induced increase in shear modulus. The higher slope of the unloading curve is puzzling. This could result from continued forward shear during the early phases of unloading and will be considered below. In the unloading reloading cycle there is no protracted plastic transition. Onset of plastic flow on reloading is quite sharp and at the old level of resistance. Finally, we note that upon reloading there is a characteristic yield phenomenon of flow stress overshoot at the plateau, while the stress reaches its plateau smoothly without an overshoot during the initial protracted transition. These manifestations are all important and clarify the nature of plastic shear flow.

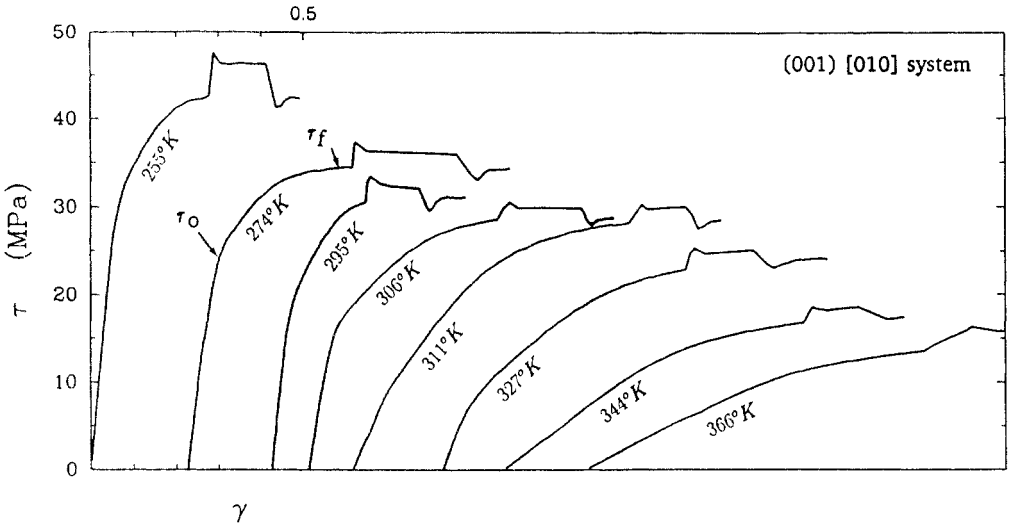

Figure 5. Stress–strain curves for the monoclinic (001)[010] chain slip system at eight different temperatures showing changes in elastic properties, CRSS, τ_0, flow stress τ_f, and effects of strain rate change by a factor of 10.

Table 1. Activation Parameters of the Monoclinic (001)[010] System[a]

T (K)	$\dot{\gamma}_1$ ($\times 10^{-3}$ s^{-1})	$\dot{\gamma}_2/\dot{\gamma}_1$	μ (MPa)	τ_0 (MPa)	τ_{f1} (MPa)	$\Delta\tau_f$ (MPa)	τ_{f2}[b] (MPa)	Δv^* ($\times 10^{-21}$ cm^3)	Δa^* ($\times 10^{-14}$ cm^2)	m
295	2.36	1	576	16.7	33.1					
295	23.60	1	586	20.1	34.9					
295	2.36	2	588	16.8	32.8	0.88	33.34			
295	2.36	5	580	16.3	32.4	2.04	33.57			
255	2.36	10	594	28.5	42.5	4.96	46.32	1.60	0.93	16.0
274	2.36	10	580	24.1	34.4	3.03	36.22	2.83	1.64	20.1
295	2.36	10	584	17.0	32.3	3.03	34.16	3.04	1.76	18.5
306	2.36	10	502	15.1	28.5	2.12	29.85	4.51	2.62	22.2
311	2.36	10	147	13.1	27.6	2.19	29.33	4.45	2.58	20.6
327	2.36	10	100	8.2	22.7	2.54	24.29	3.98	2.31	13.3
344	2.36	10	54	8.2	14.6	1.92	15.96	5.44	3.15	7.9
366	2.36	10	40	7.9	11.5	2.87	13.29	3.57	2.07	2.8

[a] τ_a = 8 MPa, athermal resistance. [b] τ_{f2} is new "steady state" flow stress at γ_2.

Similar strain rate jump experiments were performed at eight different temperatures, ranging from a low of 255 K to a high of 366 K. Figure 5 shows the stress–strain curves of these experiments with sudden changes of strain rate at their respective plateau levels from 2.36×10^{-3} to 2.36×10^{-2} s^{-1} and then back to 2.36×10^{-3} s^{-1}. The curves have been offset along the strain axis for clarity.

This figure reveals the trends in how the behavior of the (001)[010] slip system is affected by changes in temperature. It can be seen that the slopes of the elastic portions of the curves are almost unaffected by temperature below 306 K but become quite significantly reduced for temperatures starting with 311 K. The slopes drop very markedly between 306 and 344 K. It should be noted that the glass transition temperature, T_g, of the amorphous component of Nylon 6 with a low level of absorbed water is between 313 and 360 K but could be reduced with absorbed water.[26] The figure shows that the initial yield stress τ_0 and the flow stress τ_f at the flow stress plateau decrease as the temperature increases. It is also to be noted that stress overshoots due to strain rate changes are present at all eight temperatures and the stress plateaus slope slightly upward at temperature higher than 311 K.

The results of these strain rate change experiments at different temperatures are summarized in Table 1. Column 1 gives the different experimental temperatures. Column 2 gives the primary (initial) strain rates $\dot{\gamma}_1$ used in simple shear experiments prior to the sudden change. When a strain rate jump was performed, initially more than one strain rate was considered for the high strain rate. These second and higher strain rates used were 2, 5, and 10 times the first strain rate. The ratios of the two strain rates in the changes are listed in column 3. In columns 4–6 are the shear moduli μ ($=s_{66}^{-1}$), the critical resolved shear stresses τ_0, and the flow stresses τ_{f1} corresponding to the initial strain rate $\dot{\gamma}_1$, at the sudden upward change.

The data in the first four rows and in row 7 of Table 1 came from experiments at room temperature. The difference is the initial strain rates used. It can be seen that the difference in the shear modulus for the different initial strain rates at 295 K was imperceptible in the stress–strain curves. Any variation is attributed to experimental error. However, the critical resolved shear stress increased by a value between 3.1 and 3.8 MPa (about 20%), while the flow stress increased by a value between 1.8 and 2.6 MPa (about 6.9%) when the initial strain rate used was suddenly increased by a factor of 10. The critical resolved shear stresses were 16.7 MPa (average of rows 1, 3, 4, and 7) and 20.1 MPa for the initial strain rates of 2.36×10^{-3} and 2.36×10^{-2} s^{-1}, respectively. In a previous study[15] the critical resolved shear stress determined from an interpolation of tension and compression experiments was given as 16.24 MPa for a corresponding shear strain rate of about 2.36×10^{-3} s^{-1}, which is within 3% of the value measured in the present simple shear experiment. As is indicated by the data in column 7, the flow stress increased by 0.88, 2.04, and 3.03 MPa when the strain rates were changed by factors of 2, 5, and 10, respectively. The stress exponents m for strain rate (discussed further below) in column 11 are in the range of 20 for τ_f which indicates a low strain rate sensitivity of the flow stress, typical of plastic shear flow. On the other hand, considering the changes in the CRSS τ_0 for the two different strain rates at 295 K (average

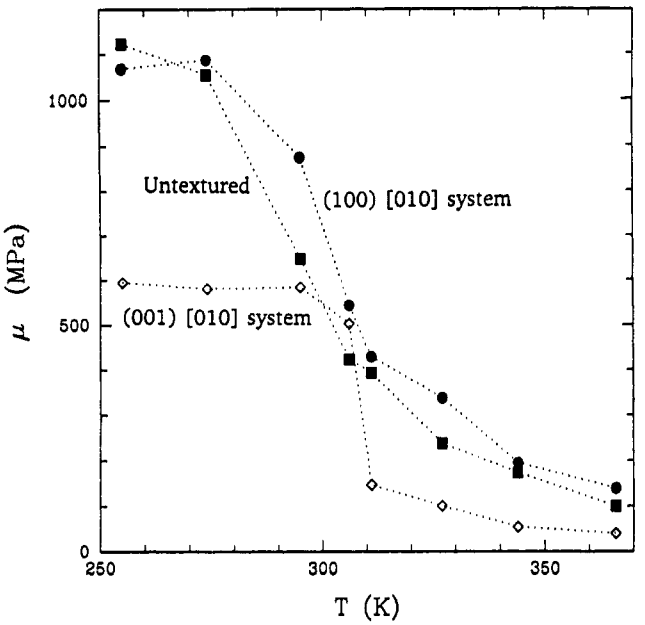

Figure 6. Temperature dependence of the shear moduli s_{66}^{-1} of the monoclinic (001)[010], s_{55}^{-1} of the orthotropic (100)[010] systems, and μ of the untextured material. In all cases there is a clear glass transition at around 310 K.

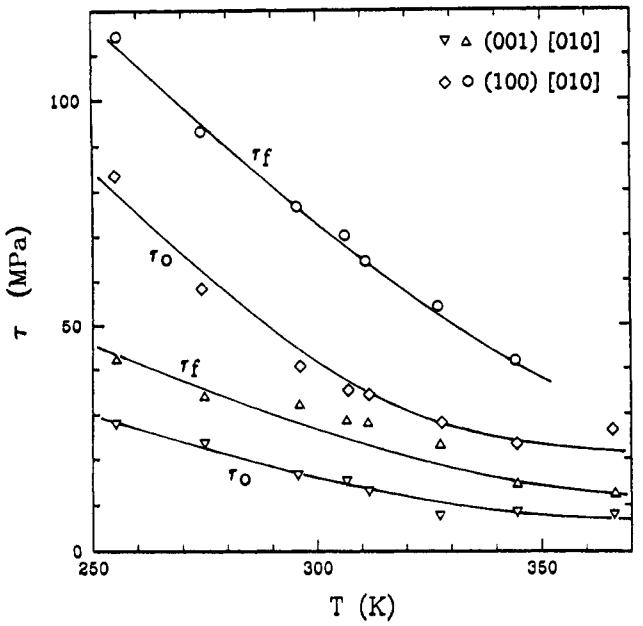

Figure 7. Temperature dependence of τ_0 and τ_f for the monoclinic (001)[010] and orthotropic (100)[010] chain slip systems showing no apparent glass transition in the plastic shear resistances.

of rows 1, 3, 4, and 7 and row 2), we calculate a stress exponent m of only 6.98 which is quite different from that for the flow stress and indicates a different mechanism that controls the CRSS.

The change of the shear modulus μ ($=s_{66}^{-1}$) with temperature is plotted in Figure 6. At low temperatures the modulus is relatively constant at 600 MPa but drops sharply down to 40 MPa in a narrow temperature range around 310 K. The change in the CRSS τ_0 and the flow stress τ_f with temperature for this chain slip system is given in Figure 7. It shows a monotonic and smooth, almost linear decrease in these resistances with increasing temperature. The CRSS levels off at 8.2 MPa around 327 K. The behavior of τ_f is similar and parallel to that of τ_0 but shows a tendency to level off at a slightly higher temperature to a level of 14.6 MPa. Neither of these two

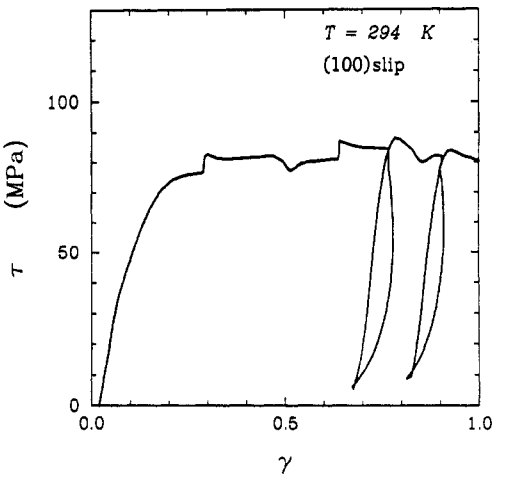

Figure 8. Typical stress–strain curve for the orthotropic (100)-[010] chain slip system at room temperature.

resistances show any sign of a sharp drop at 310 K similar to what occurs in the modulus.

3.2. Monoclinic (100)[010] Slip System. Similar simple shear experiments were conducted on the orthotropic (100)[010] slip system to probe indirectly the slanted monoclinic systems (100)[010]. Figure 8 shows a complete stress–strain curve on the orthotropic plane of an experiment performed at room temperature, with strain rate changes and two cycles of unloading and reloading. The first unloading and reloading was done at the high strain rate of 2.36×10^{-2} s^{-1}, while the second was at the low strain rate of 2.36×10^{-3} s^{-1}. Moreover, comparison of these results with those in Figure 4 for the monoclinic (001)[010] system shows a much more enhanced unloading–reloading hysteresis in the orthotropic (100)[010] system, resulting from the much more prominent curvature of the unloading curve in this system than in the former. Figure 9 gives a collection of stress–strain curves at eight different temperatures, in this orthotropic orientation, corresponding to those of the (001)[010] system given in Figure 5, showing again the effect of strain rate changes by a factor of 10. From these curves the temperature dependences of the orthotropic shear modulus, s_{55}^{-1}, the orthotropic CRSS τ_0, the orthotropic flow stress τ_f, and the stress jumps were obtained and are listed in Table 2. This information is also plotted in Figure 6 for s_{55}^{-1} and in Figure 7 for τ_0 and τ_f of the orthotropic systems.

To determine the characteristics of deformation of the monoclinic (100)[010] slip system and its activation parameters, the properties and the measured activation parameters of the orthotropic (100)[010] system were resolved on the slanted monoclinic planes, according to the following procedure:

$$\tau_{m(100)[010]} = \cos\theta\,\tau_{o(100)[010]} \quad (1)$$

$$\gamma_{m(100)[010]} = \cos\theta\,\gamma_{o(100)[010]} \quad (2)$$

$$(\mu_{m(100)[010]})^{-1} = \sin^2\theta(\mu_{m(001)[010]})^{-1} + \cos^2\theta(\mu_{o(100)[010]})^{-1} \quad (3)$$

In eqs 1–3 $\theta = 21°$ is the angle between the monoclinic and orthotropic X_3 axes, and the subscripts m and o stand for monoclinic and orthotropic, respectively. The calculated monoclinic deformation characteristics and activation parameters to be discussed below in section 4.3 are listed in Table 3.

3.3. Untextured Nylon 6. A set of simple shear experiments were also performed on previously unde-

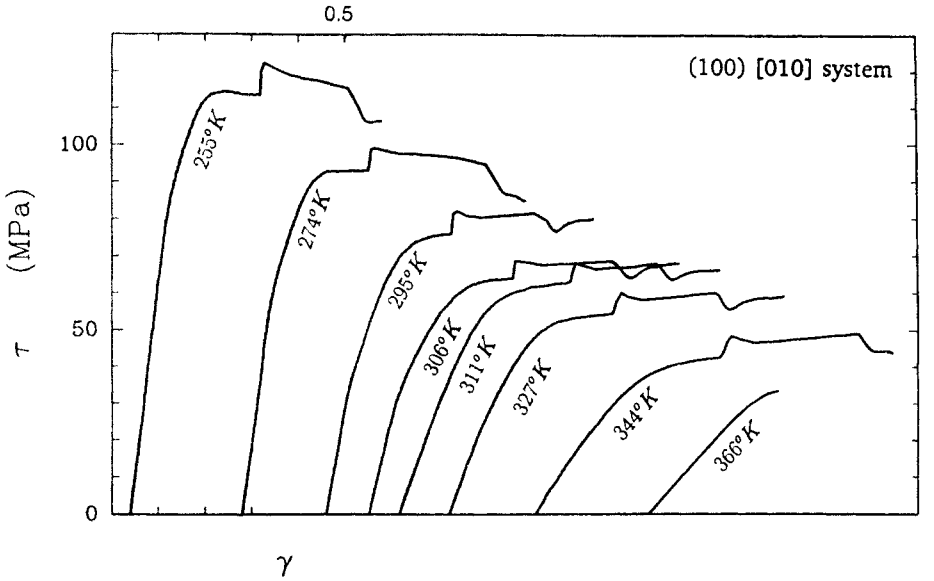

Figure 9. Temperature dependence of the stress–strain response of the orthotropic (100)[010] system at eight different temperatures showing also the effect of strain rate changes.

Table 2. Activation Parameters of the Orthotropic (100)[010] System[a]

T (K)	$\dot{\gamma}_1$ ($\times 10^{-3}$ s^{-1})	$\dot{\gamma}_2/\dot{\gamma}_1$	μ (MPa)	τ_0 (MPa)	τ_{f1} (MPa)	$\Delta\tau_f$ (MPa)	τ_{f2}[b] (MPa)	Δv^* ($\times 10^{-21}$ cm^3)	Δ_a^* ($\times 10^{-14}$ cm^2)	m
255	2.36	10	1067	81.44	113.37	6.74	118.86	1.19	0.69	30.9
274	2.36	10	1085	57.76	92.50	4.66	96.34	1.85	1.07	34.4
295	2.36	10	873	42.00	76.61	4.64	79.49	1.99	1.16	26.7
306	2.36	10	542	35.08	69.61	3.55	71.78	2.71	1.57	30.3
311	2.36	10	428	33.90	63.76	3.73	65.96	2.61	1.52	25.2
327	2.36	10	337	26.80	53.93	4.07	56.03	2.50	1.45	17.5
344	2.36	10	195	22.90	41.70	4.19	44.13	2.52	1.46	10.3
366	2.36	10	138	25.83						

[a] τ_0 = 22.9 MPa, athermal resistance. [b] τ_{f2} is new "steady state" flow stress at $\dot{\gamma}_2$.

Table 3. Activation Parameters of the (100)[010] Monoclinic System[a] (Determined from Measurements on the (100)[010] Orthotropic System)

T (K)	$\dot{\gamma}_1$ ($\times 10^{-3}$ s^{-1})	$\dot{\gamma}_2/\dot{\gamma}_1$	μ_m (MPa)	τ_m (MPa)	τ_{f1} (MPa)	$\Delta\tau_f$ (MPa)	τ_{f2} (MPa)	Δv^* ($\times 10^{-21}$ cm^2)	Δa^* ($\times 10^{-14}$ cm^2)	m
255	2.20	10	968	76.03	105.84	6.29	110.97	1.27	0.74	30.90
274	2.20	10	976	53.92	86.36	4.35	89.94	1.83	1.06	34.40
295	2.20	10	820	47.23	71.52	4.33	74.21	2.14	1.24	26.70
306	2.20	10	537	32.75	64.99	3.31	67.01	2.91	1.69	30.34
311	2.20	10	344	31.65	59.52	3.48	61.58	2.80	1.63	25.24
327	2.20	10	259	25.02	50.35	3.80	52.31	2.68	1.56	17.58
344	2.20	10	146	21.38	38.93	3.91	41.20	2.73	1.58	10.34
366	2.20	10	105	24.11						

[a] τ_a = 21.38 MPa. [b] τ_{f2} is new steady state flow stress at $\dot{\gamma}_2$.

formed (untextured) Nylon 6 for reference. A stress–strain curve of an experiment performed at room temperature is shown in Figure 10. The procedure of strain rate jump, unloading, and reloading was the same as that for the textured material. It can be seen that the yield stress τ_0 is faily low but the hardening rate is high as are the magnitudes of the stress jumps. The yield overshoots continue to be present, and the slope of reloading is very different from the slope of unloading, which is now very markedly bowed out the same as for the case of the orthotropic (100)[010] experiment. One clear difference between the untextured material and the textured one is that a stress plateau is still not reached even at a strain approaching 1.0 for the untextured material. This can also be seen from Figure 11 which collects eight stress–strain curves of simple shear experiments performed at eight different temperatures. The temperature dependence of the shear modulus and the initial yield stress of the untextured Nylon 6 is given in Figures 6 and 12, respectively. From Figure 6, it can be seen that the shear modulus of the untextured material decreases as dramatically as for the textured material but that this drop is spread over a much wider temperature range (from 275 to

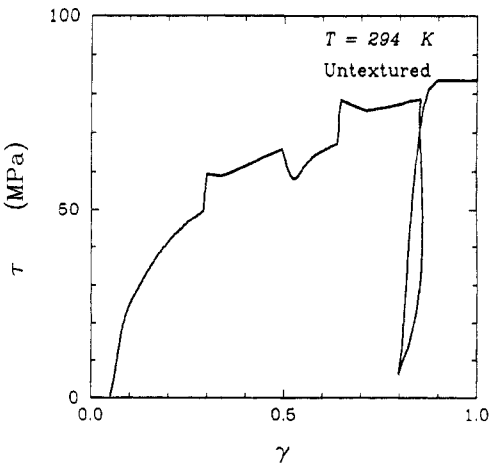

Figure 10. Typical stress–strain curve for the untextured material at room temperature.

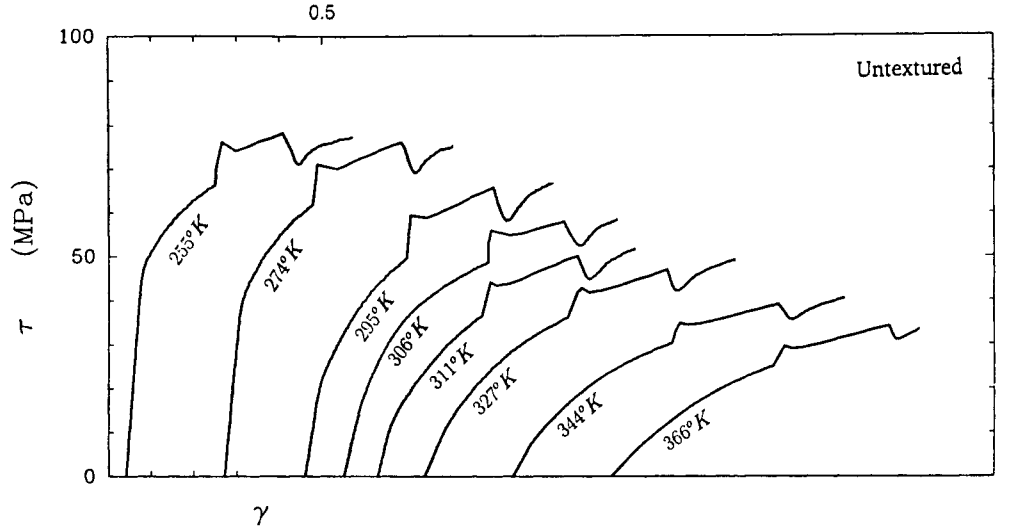

Figure 11. Temperature dependence of the stress–strain response of untextured material at eight different temperatures, showing also the effect of strain rate changes.

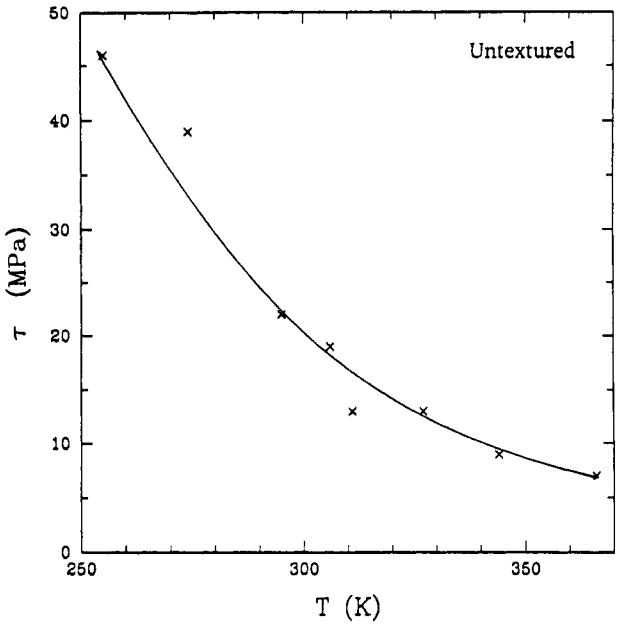

Figure 12. Temperature dependence of the CRSS τ_0 of untextured material.

350 K). Figure 12 indicates that there also exists an athermal level of deformation resistance for the untextured material, which is approximately 8 MPa. The results of activation measurements for this material are given in Table 4.

4. Discussion

4.1. Constitution of the Material. The constitution of the initially undeformed, untextured Nylon 6 is spherulitic and was described in considerable detail by Galeski et al.[20,27] We will delay discussing the simple shear response of this spherulitic material and its rate dependence to section 4.6, further below. Here we want to concentrate primarily on the deformation mode and the rate dependence of the quasi-single crystalline (QSC) material prepared initially by plane strain compression to an equivalent strain of $\epsilon_e = 1.39$. While this QSC material with its symmetrically arranged dual monoclinic domain morphology (Figure 1) does not have the same degree of perfection of its orthorhombic HDPE counterpart, described by Galeski et al.,[13] Bartczak et al.,[16] and Schönherr et al.,[17] we idealize its constitution of overall orthotropic symmetry to be similar to that of the orthorhombic HDPE. Thus, we assume that a similar degree of textural alignment in the crystalline component and quasi-crystalline molecular alignment demonstrated for HDPE[16,17] also exists in QSC Nylon 6. On the basis of the dual domain morphology depicted in FIgure 1, we expect that this correspondence is better for the principal chain slip system (001)[010] of Nylon 6 and less so for the actual inclined dual monoclinic (100)[010] chain slip system on which slip has to cut across hydrogen bonds. We concede, moreover, that the SAXS patterns in fully textured Nylon 6 are sharper than the corresponding patterns in HDPE, indicating that in the former a better defined stratification of a layered amorphous component must exist, with its corrugated layers having cylindrical generating lines parallel to the X_3 (CD) direction. Nevertheless, we assume that, as in HDPE, a sizable fraction of the amorphous component is also dispersed into the crystalline component as small inclusions of chain flipovers or slack pockets, as depicted in Figure 13. On the other hand, there is considerable evidence[12] that in the layered amorphous regions a substantial background coherence in the form

Table 4. Activation Parameters of Untextured Reference Material[a]

T (K)	$\dot{\gamma}_1$ ($\times 10^{-3}$ s^{-1})	$\dot{\gamma}_2/\dot{\gamma}_1$	μ (MPa)	τ_0 (MPa)	τ_{f1} (MPa)	$\Delta\tau_f$ (MPa)	τ_{f2} (MPa)	Δv^* (10^{-22} cm^3)	Δa^* ($\times 10^{-15}$ cm^2)	m
255	2.36	10	1123	46.06	66.20	10.27	72.37	7.69	4.46	13.1
274	2.36	10	1056	39.00	61.81	9.61	67.72	8.91	5.17	12.9
295	2.36	10	646	22.07	49.30	10.10	56.77	8.95	5.19	9.4
306	2.36	10	423	19.05	48.44	7.62	52.95	12.40	7.20	12.2
311	2.36	10	393	13.01	36.51	8.05	41.70	11.80	6.83	8.2
327	2.36	10	237	13.05	35.88	6.98	40.06	14.30	8.32	9.2
344	2.36	10	174	9.00	30.33	5.01	33.17	21.10	12.20	10.3
366	2.36	10	101	7.06	25.08	4.72	28.04	23.70	13.70	8.3

[a] $\tau_0 = 8$ MPa, athermal resistance. [b] τ_{f1} and τ_{f2} are not at a steady plateau but are the flow stresses where a strain rate change was initiated and the corresponding "equilibrium" flow stress at the new strain rate, respectively.

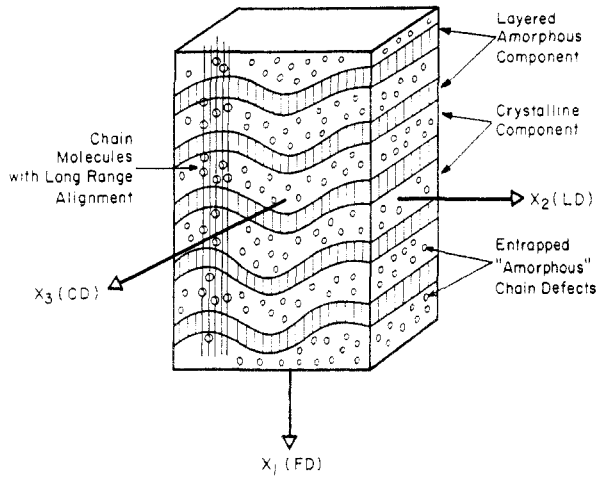

Figure 13. Sketch of the morphological constitution of the QSC material.

of transverse short range order is likely to be present, similar to what was reported for HDPE.[16] Thus, we expect that in the QSC material a large fraction of aligned and laterally ordered molecules bridge across the amorphous domains. In fact the primary reason for small-angle X-ray scattering patterns to develop would appear to be due to the lack of axial registry between aligned molecules in the otherwise laterally ordered amorphous component.[16]

We note that, while there is a very distinct glass transition in both the s_{66}^{-1} and s_{55}^{-1} moduli at around 310 K, there is no corresponding transition in either the CRSS τ_0 or the plastic resistance τ_f. For a spatial distribution of the amorphous and crystalline components as depicted in Figures 1 and 13, the above finding requires some explanation since plastic resistance of a solid usually correlates with its elastic stiffness.

We assume that at low temperatures below the observed T_g the amorphous layers and the amorphous clusters entrapped in the crystalline component have roughly the same elastic properties as the crystalline component. The elastic constants of the textured orthotropic QSC material were measured by Lin and Argon earlier.[18] Moreover, a decomposition of the contribution of the amorphous and crystalline components to those of the overall anisotropic elastic properties has been attempted by Hsia et al.[28] with a finite element model based on the layered distribution of the two components shown in Figure 13. Since their primary concern was to explain the elastic properties of drawn Nylon fibers requiring assumptions that are in conflict with the constitution of the QSC material used here, their findings are not directly applicable here to our morphology. Nevertheless, in a conventional interpretation of the properties of the QSC material the absence of a transition in the plastic resistance is puzzling, as already remarked above. We explain this by noting that the linear elastic stretch in the amorphous component is finite and that prior to exhibiting plastic behavior in the simple shear experiment the amorphous component must be assumed to be fully stretched out and locked.

We note further that the layered amorphous component and the dispersed amorphous clusters must have rather different characteristics. We idealize the amorphous clusters as small regions of chain disorder, entrapped in the crystalline component, that are too small and have too few unconstrained kinematical degrees of freedom to undergo a glass transition. This is in keeping with recent molecular level simulations of the processes of a glass transition in a glassy vinyl polymer such as polypropylene.[30] From such simulations it can be concluded that much like the process of plastic shear transformations, in a glassy polymer,[29] structural relaxations characteristic of a glass transition can only occur in volume elements larger than ca. 10 nm.[30] Thus, we conclude that the glass transition observed in the elastic properties of the QSC material (Figure 6) comes principally from the layered amorphous component and not from the small disordered "amorphous" clusters which behave as elastic inhomogeneities in the crystalline component. To reiterate our statement above, we assume that at the onset of plastic shear flow the layered amorphous component is fully "stretch polarized" and has a high degree of lateral order with molecular continuity to the attached crystalline layers.

Thus, for the purpose of interpreting our rate mechanism measurements we idealize our QSC Nylon as being made up of a coherent quasi-single crystalline background of molecules with a high degree of long range coherent arrangement of the principal (001)[010] chain slip systems over both the crystalline and amorphous components. We expect that a certain fraction of the amorphous component is dispersed into the crystalline component in the form of small clusters as chain crossovers, double kinks, slack molecular segments, etc., acting as misfitting inhomogeneities, and incapable of undergoing a glass transition. While we have no information on the size of the bimodally distributed domains of monoclinic crystallites depicted in Figure 1, we will assume that there exists a similar degree of long range coherence of the (100)[010] monoclinic systems.

4.2. Plastic Response of Chain Slip. In what follows we will interpret our activation measurements derived from simple shear experiments on the monoclinic (001)[010] and the (100)[010] chain slip systems of the QSC material as being related to kinetics of screw dislocation motion in the coherent background quasi crystal of long range coherence. In this we begin by noting that in a perfect monoclinic crystal the mobility of edge dislocations on both the (001)[010] and the (100)[010] chain slip systems should be much higher than screw dislocations. We base this on the expectation that in view of the far higher tensile stiffness of molecules over their bending stiffness the cores of edge dislocations should be much more extended than those of screws resulting in a much lower lattice resistance to edge dislocation motion in comparison with screw motion.

Because of the dispersed clusters of amorphous material as structural misfit, we expect that there exists in the QSC material a substantial level of random internal misfit stress having a wavelength on the order of the amorphous cluster spacing, i.e., a large fraction of the long period measured in SAXS experiments. We expect that those long range misfit stresses are the principal cause of the high temperature athermal resistance τ_a given in Figure 7, impeding the motion of both edge and screw dislocations alike. The dispersed amorphous clusters, however, act also on the short range as thermally penetrable discrete obstacles. We envision that, when a dislocation line presses against an amorphous cluster made up of a chain crossover or the conformational irregularity of local molecular packing, it will be held up at the cluster, while other adjoining segments bow out between clusters as depicted in Figure 14. We assume that in most instances it is kinematically possible for the dislocation to force some momentary order in the cluster to permit it to overcome the cluster without any bond rupture, resulting in the restoration of a similar conformational disorder in the amorphous region upon the passage of the dislocation. We assume that such shearing and overcoming of amorphous clusters can be

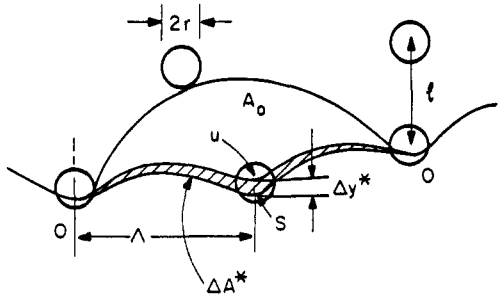

Figure 14. Dislocation bowing through disordered clusters.

thermally assisted, and therefore it is the principal cause of the temperature dependence of τ_f. On the basis of the constitution of the QSC material described in section 4.1 above, we expect the temperature dependence of the elastic properties to affect only the "stretch polarization" of the material in simple shear but not its plastic properties.

To begin, as already stated, we expect the random misfit stresses due to the entrapped small clusters of disorder to result in an athermal resistance τ_a to dislocation motion similar to the athermal threshold of solid solution, strengthening the mechanism of which was described by Mott and Nabarro[31] (for a recent description of this process under the label of "Mott statistics", see Kocks et al.[32]). Thus, at elevated temperatures the entire resistance to the inception of plastic behavior is considered to be a result of the long range effect of these misfit stresses, which we take to be 8 MPa (while the lowest levels of τ_f in Figure 7 are around 14 MPa for the high temperature experiments, since a negative slope is discernable in τ_f at this level we have taken τ_a = 8 MPa as a likely extrapolated value) for the (001)[010] system, and the untextured material, and 21.38 MPa for the monoclinic (100)[010] system—with the substantial difference of the chain slip systems being a consequence of elastic anisotropy (Figure 6).

With decreasing temperature τ_o, the CRSS, rises above the athermal threshold τ_a. We attribute the increment of τ_o above τ_a to a lattice resistance, experienced, most probably, only by screw dislocations. This resistance ($\tau_o - \tau_a$) rises monotonically with decreasing temperature.

Figures 3–5 for the (001)[010] chain slip system and Figures 8 and 9 for the orthotropic (100)[010] chain slip system (and by inference also for the corresponding monoclinic system) show that there is a substantial amount of apparent hardening between the inception of deformation and steady state flow at a stress τ_f. Rather than a conventional process of strain hardening due to the accumulation of dislocations, we view this process as a very expanded transition in the QSC material from elastic to fully developed plastic behavior. In this process the preexisting field of the shorter range component of the internal misfit stresses is systematically compensated and neutralized by dislocations that percolate through this field and are laid down as arrangements of misfit relief dislocations. We note that very substantial amounts of plastic shear strain are involved in this transition—typically on the order of 0.2. From the well-known kinematical equation of plastic strain increment $\Delta\gamma$ due to the development of a slipped area increment Δa in a volume V, i.e.,[33]

$$\Delta\gamma = b\Delta a/V \tag{4}$$

where we take $V = Ah$ and where b = 17.24 Å and h = 7.4 Å (the interplanar spacing for the (001)[010] system), we estimate $\Delta a/A$ to be roughly 8.6% of all the available area (including every adjacent plane). Normally, in crystal plasticity such a uniform distribution of slip is not possible because of mutual arrest of dislocations at considerable distances. In the QSC material, however, the conditions are quite different. For this material, for the (001)[010] system the shear modulus s_{66}^{-1} is 600 MPa, while the plastic shear resistance τ_f is 33 MPa, or larger in the same range. Thus, from the relation for the critical arrest spacing H for edge dislocations[33]

$$H = \frac{\mu b}{8\pi(1-\nu)\tau_f} \tag{5}$$

we obtain, for $\nu = 0.3$, H = 17.8 Å, or slightly over 2 spacings of (001) planes. Thus, we conclude that not only is such dense slip coverage possible but it must be accompanied by a large rate of mutual annihilation of blocking dislocations—accounting for the negligible strain hardening at τ_f. That the systematic leveling of internal stress has been very effectively accomplished during the transition range to fully developed plasticity is clear from the sharp unloading and reloading behavior demonstrated in Figure 4 for the (001)[010] system. Figure 8 shows that the same set of processes occur also for the orthotropic (100)[010] system, but somewhat less effectively so.

4.3. Dislocation Model of Plastic Shear Resistance τ_f of the QSC Material. For the purpose of analyzing the rate mechanism of plastic shear flow at the stress τ_f, we adopt well-known formalisms of precipitate strengthening[32] and consider the rather idealized picture of Figure 14 showing a dislocation line hung-up in equilibrium in the field of the inhomogeneity clusters of radius $2r$ and mean spacing l. The dislocation line segment OSO is pressed against such an obstacle under an effective shear stress of $\tau_f - \tau_a$ and bows out around it in stable equilibrium. If the dislocation segment could be thermally assisted over the obstacle to the saddle point configuration of OUO, it would be free to sweep out an area A_0(= $(\sqrt{3}/2)l^2$) and touch, on the average, just another obstacle. Then, the average distance of advance λ of the segment is given as

$$\lambda = \frac{A_o}{\Lambda} = \frac{\sqrt{3}l}{2}\left(\frac{(\tau_f - \tau_a)bl}{2\mathcal{E}}\right)^{1/3} \tag{6}$$

where

$$\Lambda = l\left(\frac{2\mathcal{E}}{(\tau_f - \tau_a)bl}\right)^{1/3} \tag{7}$$

also shown in Figure 14 as the mean unsupported dislocation segment length, is taken as the so-called Friedel sampling length.[32] In these equations b (=17.24 Å) is the length of the Burgers vector of a perfect dislocation, and $\mathcal{E} \simeq \mu b^2/2 = b^2/2s_{66}$ is the dislocation line energy (=line tension). If the free energy barrier between the stable equilibrium shape OSO and the saddle point shape OUO of the segment is ΔG^*, the shear strain rate can be given as

$$\dot{\gamma} = b\rho_m\lambda\nu_G \exp(-\Delta G^*/kT) \tag{8}$$

where ρ_m is the mobile dislocation density and ν_G is an attack frequency, usually taken as a normal mode frequency of the inhomogeneity cluster in the forward shear direction.

While the activation free energy ΔG^* with its stress dependence is not readily determinable, its features, i.e., the activation volume Δv^*, activation area Δa^*, activation distance Δy^*, are relatively simply accessible through the

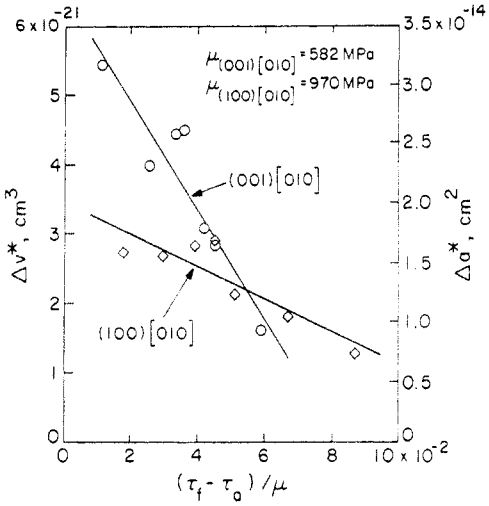

Figure 15. Dependence of Δv^* and Δa^* on stress for the monoclinic (001)[010] and the (100)[010] slip systems.

strain rate change experiment and are[32](in the determination of Δv^*, Δa^*, and Δy^*, we have ignored the possible stress dependence of Λ which if included would make the activation areas 50% larger)

$$\Delta v^* = -\left(\frac{\partial \Delta G^*}{\partial(\tau_f - \tau_a)}\right)_{p.T.} = kT\left[\left(\frac{\partial \ln\dot{\gamma}}{\partial \tau_f}\right)_{p.T.} - \frac{1}{3(\tau_f - \tau_a)}\right] \quad (9)$$

$$\Delta a^* = \Delta v^*/b \quad (10)$$

$$\Delta y^* = \Delta a^*/\Lambda \quad (11)$$

The activation volumes, and activation areas, calculated according to eqs 9 and 10 for the monoclinic (001)[010] and the (100)[010] chain slip systems are given in columns 9 and 10 of Tables 1 and 3. The dependences for the two chain slip systems are also plotted in Figure 15 as a function of the appropriate effective stresses $(\tau_f - \tau_a)$ normalized with the appropriate low temperature shear moduli which remain effective in governing the elastic interactions in the crystalline component.

Examination of the linear dependence of the activation volume or activation area on effective stress in Figure 15 indicates that they go to zero roughly at $(\tau_f - \tau_a)/\mu$ of 0.082 and 0.142 for the two monoclinic chain slip systems (001)-[010] and (100)[010], respectively. These are extremely high terminal resistances and become even higher if we recall that they are coming from the shear resistance of the dispersed amorphous inclusions which most probably have a volume fraction of no higher than about 0.25–0.33.

In the low stress limit the activation area should become comparable to A_0, the area on the slip plane allocated to one disordered obstacle. For $A_0 = (\sqrt{3}/2)l^2$, based on a hexagonal packing of the disordered obstacles in the slip plane, we estimate the mean spacing l of such obstacles to be about 2.0 nm on the (001) plane and about 1.35 nm on the (100) plane. These spacings are quite small and imply a high areal density of disordered regions which may not be fully compatible with the assumed degree of perfection of the QSC material. A considerably different interpretation can be reached if we recall that in the determination of the activation area we used the full Burgers vector of 17.24 Å for a perfect dislocation based on the repeat distance of the hydrogen bonds in the (001) plane. If we had used instead the repeat distance along the chain of the appropriate CH_2 groups as a partial dislocation, then the Burgers vector of this partial would be only 2.46 Å and the activation areas would be 7 times larger, giving for the mean spacing of the disordered regions a dimension of 5.29 nm in the (001) plane and 3.57 nm in the (100) plane, respectively. These dimensions are more in keeping with the assumed perfection of the QSC material and are consistent with the degree of perfection recognizable by atomic force microscopy in the corresponding case of highly textured high density polyethylene.[17] Clearly, a more precise interpretation of the activation parameters requires more precise information on the constitution of the QSC material and the atomic details of the structures of dislocation cores in the monoclinic lattice of Nylon 6. Neither of this information currently exists.

4.4. Mobile Dislocation Density. In activation analyses of the type we presented above it is usually assumed that dislocation generation is not difficult, that dislocation densities adjust to new needs readily, and that they are independent of stress. The "yield overshoots" in the stress–strain curves following an abrupt strain rate change indicate otherwise. At the instant of the strain rate change it is clear that the existing dislocation density is maintained and these dislocations are forced to move faster. Thus, in our thermal analysis the change in flow stress responding to the change in strain rate was taken as the difference between the starting flow stress level τ_{f1} to the yield peak. Soon after, however, an increase in the dislocation density occurs and the flow stress drops to a new level τ_{f2}, in equilibrium with the new strain rate $\dot{\gamma}_2$. These new levels of flow stress are also listed in Tables 1–4 in columns 8. We can make an estimate of the changes in mobile dislocation density by utilizing eqs 6, 8, and 9 and making a Taylor expansion of the stress dependence of the activation free energy around the initial state before strain rate change is imposed, i.e.

$$\Delta G^* = \Delta F^*(\tau_f) - (\tau_f - \tau_a)\Delta v^* \quad (12)$$

From this we obtain

$$\frac{\rho_{m2}}{\rho_{m1}} = \left(\frac{\dot{\gamma}_2}{\dot{\gamma}_1}\right)\left(\frac{\tau_{f1} - \tau_a}{\tau_{f2} - \tau_a}\right)^{1/3} \exp\left(-\frac{(\tau_{f2} - \tau_{f1})\Delta v^*}{kT}\right) \quad (13)$$

Considering a typical case for the (001)[010] system at room temperature, we obtain from eq 13 $\rho_{m2}/\rho_{m1} = 3.1$. This is a substantial fraction of the steady state response to the strain rate change.

Comparing the unloading and reloading responses of the two chain slip systems (001)[010] and (100)[010] in Figures 4 and 8, we note a much more pronounced hysteresis effect in the latter in comparison with that in the former. This becomes more puzzling considering that the stress sensitivity of the strain rate of the latter system is substantially higher than that of the former, making it quite unlikely that the forward strain bulges in the latter can be attributed to substantial continued plastic flow during unloading. Considering that the flow stresses of the latter system are more than a factor of 2 higher than those of the former, it is possible that this difference is due to an experimental artifact.

In closing this section we remark again that for both of the chain slip systems at the plateau level of flow there is negligible strain hardening. This, as already stated, is a consequence of the very substantially high ratio of the flow stress to the appropriate modulus, indicating that the mutual arrest distances of dislocations are no larger than two interplanar spacings as indicated by the analysis in connection with eq 5. Thus, mutual annihilation of

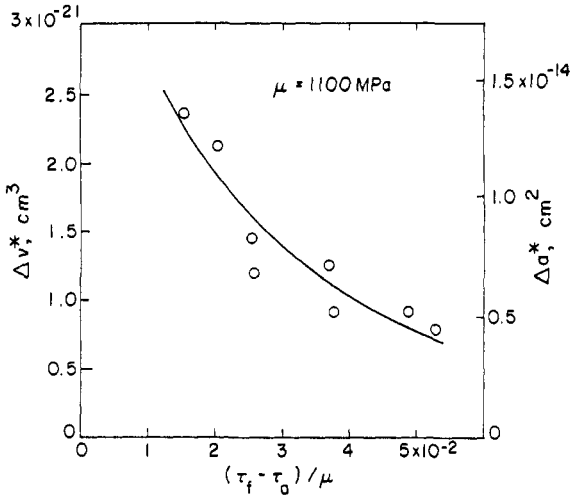

Figure 16. Dependence of Δv^* and Δa^* on stress for the untextured material.

opposite dislocations, whether of edge or screw nature, must be very high.

4.5. Lattice Resistance. As stated above we interpret the CRSS τ_0 as being due to a lattice resistance to the motion of dislocations, and possibly only screw dislocations, since edge dislocation cores are likely to be substantially wider, making them less subject to a lattice resistance.[34] Since the apparent hardening rate is quite high at the beginning of deformation, it is not effective to perform strain rate change experiments in this range to explore the activation parameters. Therefore, we limit our observation to the strain rate dependence of τ_0 obtained from different samples at room temperature, i.e., information from rows 1 and 2 in Table 1. Using eq 9 in which we interpret τ_f as τ_0, we obtain for the activation volume $\Delta v_0^* = 2.6 \times 10^{-21}$ cm^3 which is 14% smaller than the activation volume obtained from the strain rate change experiment on τ_f. Converting this to an activation area for a Burgers vector of 17.24 Å gives $\Delta a_0^* = 1.51 \times 10^{-14}$ cm^2 and an activation length of 8.76×10^{-8} cm. For motion of partial dislocations with Burgers vector 2.46 Å these latter parameters become 1.06×10^{-13} cm^2 and 4.29×10^{-6} cm, respectively. From this we can conclude that, while attributing τ_0 to a lattice resistance is reasonable, the activation parameters determined from the strain rate dependence of τ_0 make these parameters only marginally different from those determined from the response to strain rate change of τ_f. Clearly, if τ_0 were indeed due to a lattice resistance, it must then interact strongly with the assumed centers of internal misfit stress that was assumed to be responsible for τ_f. Once again better understanding necessitates better knowledge of the lattice resistance mechanism which could be obtained from direct atomistic simulation of the cores of dislocations in the monoclinic Nylon 6 lattice.

4.6. Rate Mechanism of the Untextured Material. Performing an activation analysis for the untextured material similar to the chain slip systems of the QSC material has resulted in activation volumes and activation areas (for the same long Burgers vector of 17.24 Å) that are listed in Table 4 in columns 9 and 10. The corresponding graphical information on the dependence of the activation parameters on effective stress is given in Figure 16. The figure shows that the dependence of Δv^* on $\tau_f - \tau_a$ is clearly nonlinear. When the results on this material are compared with those of the chain slip systems, we find interesting differences.

We note that the stress dependence of the plastic strain rate is low, even lower than that for the principal chain slip system (001)[010]. This, of course, is a direct consequence of the substantially smaller activation volumes (smaller by a factor of about 2) that were measured for this system as a quick perusal of Figures 15 and 16 will show. The athermal threshold resistance τ_a of the untextured material, however, is a 8 MPa, as low as that of the principal chain slip system. On the other hand, the shear modulus is as high as that of the orthotropic (100)-[010] system. The stress–strain curve in Figure 10 shows substantial hardening behavior or an expanded transition into fully developed plastic behavior with terminal flow stresses of a similar magnitude as those for the orthotropic (100)[010] system. The unloading and reloading behavior also shows considerable hysteresis, but less so than for the (100)[010] system—indicating that the behavior of the system shown in Figure 8 must represent genuine behavior. Thus, in many respects the untextured material demonstrates properties that are a mixture of the two chain slip systems. We note, however, that for even this composite behavior the temperature dependence of the flow stress shows no transition reflective of its elastic properties. Hence, our previous assumptions that were designed to explain the chain slip processes by crystal plasticity continue to hold. The elastic response of the structure continues to be stretch-polarized out before the plastic response sets in.

Clearly, the arguments of long range coherence of crystalline-like order that exists in the QSC material, which were invoked to analyze the rate mechanism there, are inapplicable for the untextured, initially spherulitic, material where the crystalline component is in the form of thin crystalline lamellar regions. Under these conditions the nature of the intervening amorphous material is of key importance in permitting, or not permitting, long range slip activity. Since the latter is quite likely, it will be necessary to consider crystal plasticity in small narrow domains linked to other such domains through ill-defined border conditions. This remains, mechanistically, as an important topic for further consideration. In the overall texture evolution simulations performed by Parks and associates,[35-37] whose work was closely associated with the present study, the problem has never surfaced, since in their computer simulations viewing the material as a polycrystalline continuum, with attached crystalline and amorphous layers, the scale of the volume elements in which plasticity is considered does not need to be defined, while mechanistically this is of vital importance. Nevertheless, the simulations of Lee et al.[37] have been quite successful in predicting most of the aspects of the deformation process.

5. Conclusions

The rate mechanisms of crystal plasticity on the monoclinic (001)[010] and the orthotropic (100)[010] chain slip systems (and by resolution also on the monoclinic (100)[010] system) of Nylon 6 in α form have been measured in simple shear experiments on quasi-single crystalline (QSC) textured material prepared earlier by plane strain compression in a channel die. In the latter system shear has to cut across hydrogen bands. The determination of activation parameters was carried out by means of strain rate change experiments between 255 and 366 K. Additional simple shear experiments were also performed on previously untextured samples of Nylon 6 for comparison.

In the QSC material, after a transition to fully developed plastic flow is complete, involving a shear strain on the

order of 0.2, flow on the chain slip systems continues with negligible hardening to large strains.

Experiments show that, while the shear moduli of both the textured and untextured material undergo a glass transition aroun 310 K, the decrease in the plastic shear resistances is smooth and monotonic, without an abrupt transition, indicating that the rate-controlling process in plasticity resides in the crystalline component.

Activation volumes determined from the strain rate change experiments were found to be stress dependent, as expected, giving an extrapolated 0 K threshold resistance for the chain slip systems of 8.2% and 14.2% of the respective shear moduli for the two monoclinic chain slip systems (001)[010] and (100)[010].

The activation volumes at low stress were found to be 6×10^{-21} cm^3 for the (001)[010] system and 2×10^{-21} cm^3 for the (100)[010] system and 2.37×10^{-21} cm^3 in the untextured material. The activation areas determined from these measurements suggest that the rate-controlling obstacles are most probably small disordered regions of chain defects similar to those in the QSC material having a spacing in the active slip planes between 2 and 7 nm depending upon whether shear is produced by perfect or by partial dislocation of Burgers vectors 17.24 or 2.46 Å, respectively.

The critical resolved shear stress τ_0 that has been measured for the chain slip systems is attributed to a lattice resistance to the motion of screw dislocations in the QSC material.

The apparent hardening between τ_0 and τ_f is considered not to be a classical process of strain hardening but as a spread out transition to fully developed plasticity during which the misfit stresses due to chain disorder are systematically neutralized by preferential stacking of dislocations acting as misfit relief dislocations.

An athermal threshold shear resistance is found for all systems at elevated temperatures where the lattice resistance becomes negligible. This athermal shear resistance was taken to be 8 MPa for the monoclinic (001)[010] system and the untextured material and 21.38 MPa for the monoclinic (100)[010] system. It has been attributed to the long range component of the disorder related misfit stresses acting on dislocations similar to a temperature-independent solid–solution plateau resistance.

Acknowledgment. This research has been supported by a DARPA U.R.I. program under ONR Contract No. N00014-86-K-0768.

References and Notes

(1) Peterlin, A. *J. Mater. Sci.* **1971**, *6*, 490.
(2) Ward. I. M. *J. Mater. Sci.* **1971**, *6*, 1397.
(3) Keller, A.; Pope, D. P. *J. Mater. Sci.* **1971**, *6*, 453.
(4) Lin, L.; Argon, A. S. *J. Mater. Sci.* **1994**, *29*, 294.
(5) Predecki, P.; Statton, W. O. *J. Appl. Phys.* **1966**, *37*, 4053.
(6) Predecki, P.; Statton, W. O. *J. Appl. Phys.* **1967**, *38*, 4140.
(7) Li, J. C. M.; Gilman, J. J. *J. Appl. Phys.* **1970**, *41*, 4248.
(8) Peterson, J. M. *J. Appl. Phys.* **1966**, *37*, 4047.
(9) Shadrake, L. G.; Guiu, F. *Philos. Mag.* **1976**, *34*, 565.
(10) Shadrake, L. G.; Guiu, F. *Philos. Mag.* **1979**, *39*, 785.
(11) Mandelkern, L. In *Crystallization of* Polymers; Dosiere, M., Ed.; NATO Advanced Study Institute Series C405; Kluwer Academic Publishers: Brussels, Belgium, 1993; p 25.
(12) Galeski, A.; Argon, A. S.; Cohen, R. E. *Macromolecules* **1991**, *24*, 3953.
(13) Galeski, A.; Bartczak, Z.; Argon, A. S.; Cohen, R. E. *Macromolecules* **1992**, *25*, 5705.
(14) Bartczak, Z.; Argon, A. S.; Cohen, R. E. *Macromolecules* **1992**, *25*, 5036.
(15) Lin, L.; Argon, A. S. *Macromolecules* **1992**, *25*, 4011.
(16) Bartczak, Z.; Galeski, A.; Argon, A. S.; Cohen, R. E. *Polymer*, in press.
(17) Schönherr, H.; Vancso, G. J.; Argon, A. S. *Polymer*, in press.
(18) Young, R. J.; Bowden, P. B. *J. Mater. Sci.* **1973**, *8*, 1177.
(19) Song, H. H.; Argon, A. S.; Cohen, R. E. *Macromolecules* **1990**, *23*, 870.
(20) Galeski, A.; Argon, A. S.; Cohen, R. E. *Macromolecules* **1988**, *21*, 2761.
(21) Lin, L. An Experimental Study of Deformation Mechanisms and Resistances of Semi-Crystalline Polymers; Ph.D. Thesis, Department of Mechanical Engineering, Massachusetts Institute of Technology, Cambridge, MA, 1991.
(22) G'Sell, C.; Boni, S.; Shrivastava, S. *J. Mater. Sci.* **1983**, *18*, 903.
(23) Robertson, R. E.; Johnson, C. W. *J. Appl. Phys.* **1966**, *37*, 3969.
(24) Robertson, R. E. *J. Polym. Sci., Polym. Phys. Ed.* **1969**, *7*, 1315.
(25) Brown, N.; Duckett, R. A.; Ward, I. M. *Philos. Mag.* **1968**, *18*, 483.
(26) Branrup, J.; Immergut, E. *Polymer Handbook*, 3rd Ed.; John Wiley & Sons: New York, 1989.
(27) Galeski, A.; Argon, A. S.; Cohen, R. E. *Makromol. Chem.* **1987**, *188*, 1195.
(28) Hsia, K. J.; Xin, Y.-B.; Lin, L. *J. Mater. Sci.* **1994**, *29*, 1601.
(29) Mott, P. H.; Argon, A. S.; Suter, U. W. *Philos. Mag.* **1993**, *67*, 931.
(30) Sylvester, M. Molecular Dynamics Studies of the Liquid–Glass Transition in Atactic Poly(propylene). Ph.D. Thesis, Department of Mechanical Engineering, Massachusetts Institute of Technology, Cambridge, MA, 1992.
(31) Mott, N. F.; Nabarro, F. R. N. *Report of a Conference on the Strength of Solids*; Physical Society: London, 1948; p 1.
(32) Kocks, U. F.; Argon, A. S.; Ashby, M. F. *Progress in Materials Science*; Chalmers, B., Christian, J. W., Massalski, T. B., Eds.; Pergamon Press: Oxford, 1975; Vol. 19, p 58.
(33) McClintock, F. A.; Argon, A. S. *Mechanical Behavior of Materials*; Addison-Wesley: Reading, MA, 1966.
(34) Foreman, A. J.; Jaswon, M. A.; Wood, J. K. *Proc. Phys. Soc.* **1951**, *A64*, 156.
(35) Parks, D. M.; Ahzi, S. *J. Mech. Phys. Solids* **1990**, *38*, 701.
(36) Lee, B. J.; Parks, D. M.; Ahzi, S. *J. Mech. Phys. Solids* **1993**, *41*, 1651.
(37) Lee, B. J.; Argon, A. S.; Parks, D. M.; Ahzi, S.; Bartczak, Z. *Polymer* **1993**, *34*, 3555.